44th AIAA/ASME/ASCE/AHS Structures, Structural Dynamics, and Materials Confere
7-10 April 2003, Norfolk, Virginia

AIAA 2003-1612

SIZE AND STRAIN RATE EFFECTS IN TENSILE DEFORMATION OF CU NANOWIRES

Wuwei Liang and Min Zhou†

The George W. Woodruff School of Mechanical Engineering
Georgia Institute of Technology, Atlanta, GA 30332-0405, U.S.A.

ABSTRACT

MD simulations with an embedded atom method (EAM) potential is used to analyze the size and strain rate effects on the tensile deformation of Cu nanowires. The nanowires are single-crystals with axes in the [001], [010], and [001] directions. The cross-sectional dimensions of the nanowires vary from 5-20 lattice constants (or 1.8-7.2 nm). The length of the specimens is 60 lattice constants (or 21.6 nm). Deformations under constant strain rates between 1.67×10^{7} s^{-1} and 1.67×10^{9} s^{-1} are analyzed. The variation of yield stress with specimen size and deformation rate is studied. It is found that the yield stress (stress at which plastic deformation initiates) decreases with specimen size, while increases with loading rate. On the other hand, ductility (strain at which total separation occurs) increases with specimen size and strain rate. The influences of specimen size are a result of enhanced opportunities for dislocation motion at larger sizes. The influences of strain rate are due to the dynamic wave effect or phonon drag that impedes the motion of dislocations. The analysis also focuses on the variation of deformation mechanisms with specimen size and strain rate. There is a clear transition in deformation mechanism as specimen size is changed. Specifically, when cross-sectional dimensions are on the order of only a few lattice constants, a combination of twinning and slip is observed. At larger cross-sectional sizes (10-20 lattice constants), crystalline slip is primarily responsible for the progression of plastic deformation. A strong strain rate effect is also seen. As strain rate is decreased, a transition of deformation mechanism from combined twining, and slip to sequential propagation of slip along well defined and favorably oriented slip planes is observed. At the lower strain rates, a well-structured activation of slip on alternating slip planes is the primary deformation mode. As the deformation of nanowires is an intrinsically dynamic process. Proper distinction between internal stress and externally applied stress (traction) must be made. In the current analysis, both the internal stress and externally applied traction are tracked. Historically, Virial stress is widely used to calculate stress in an MD system. The virial stress a kinetic energy part and an interatomic force part. Zhou (2002) has shown that the interatomic force part of the virial stress alone fully constitutes the Cauchy stress. This new understanding is reflected and used in this paper. In particular, the analysis focuses on the level of errors that may be caused in stress calculation when the kinetic energy term is included. It is found that the relative error varies as the deformation progresses. At the onset of yielding, the level of error is on the order of 5-10%. However, at large plastic strains, the error is typically of the order of 30% and can exceed 100% toward late stages of deformation when fracture initiates.

I. INTRODUCTION

The deformation of nanowires and atomic systems at finite temperatures in general is an intrinsically dynamic process. Size and strain rate effects arise out of several factors and play important roles in determining the response of nanostructures. For example, the behavior and properties of nanowires are size-dependent due to the discreteness of atomic structures, the length scale (or spatial range) of the atomic interactions, lattice structure, and lattice size scale. The dynamic inertia effect and the finite speeds at which lattice waves propagate also introduce length scales to the problem and contribute to size-dependence of atomic behavior. The inertia effect and finite wave speeds, along with phonon effects, also cause the response of nanostructures to be deformation-rate dependent.

Experimental and numerical studies have been conducted and reported in recent years [1-4]. For example, Lu et al. (2001) observed that the ductility of nano-

† To whom correspondence should be addressed, Tel: 404-894-3294, Fax: 404-894-0186,
Email: min.zhou@me.gatech.edu

crystalline Cu specimens increases as strain rate increases in experiments[5]. This strain rate dependence of ductility is completely different from that observed in coarse-grained Cu, where the fracture strain decreases with increasing strain rate. Ikeda et al. (1999) and Branício and Rino (2000) used molecular dynamics (MD) simulations to study the amorphization in metallic nanowires under high strain rates[6, 7]. They found that at strain rates lower than 7×10^{10} s^{-1}, the nanowires undergo plastic deformation in their crystalline structure and exhibit superplasticity. On the other hand, at strain rates equal to or higher than 7×10^{10} s^{-1}, the nanowires undergo a phase transition from a crystalline structure to an amorphous state. Horstemeyer and Baskes (1999) analyzed the effects of size and time scale on the plastic deformation of bulk single crystal Cu under shear loading[8]. They found that samples with less than ~1000 atoms showed little dependence of failure stress on strain rate. This is because small samples do not provide opportunities for plastic deformation to occur through coordinated slip or dislocation motion. Consequently, the deformation is primarily elastic. On the other hand, for larger samples they found at relatively small strain rates, the yield stress is independent of strain rate, while at higher strain rates the yield stress increases rapidly. This effect is attributed to the fact that multiple dislocations are nucleated at the higher strain rates, lowering the yield stress. They also asserted that four regions of bulk plastic behavior exist based upon the size scale of the solid medium. As the size scale increases, there is a gradual change of influence on plastic behavior from dislocation nucleation at much smaller scales to dislocation density and distribution at larger scales.

Historically and even presently, MD calculations of the mechanical response of atomic systems have been almost exclusively carried out at very high strain rates which are above 10^9 s^{-1}. This is primarily out of necessity. Specifically, the time steps allowable in MD calculations are limited by the need to resolve high frequency thermal oscillations for atoms and are quite small (on the order of 1 femtosecond). High rates of deformation allow high levels of strain to be reached with practically available computer resources. The use of high deformation rates introduces several issues. First, direct comparisons with experiments are extremely difficult to justify since it is so far not possible to conduct controlled laboratory experiments at high strain rates on nanowires or nano-structures. The artificially high rates also have necessitated computational schemes that allow computations to proceed. One issue is temperature control. Many authors have carried out MD simulations of nanowires using the Nose-Hoover thermostat scheme[9, 10] or the velocity scaling scheme which keep the temperature at constant values. If such schemes were not used, the artificially high strain rates would lead to temperatures over the melting point of the system under consideration, invalidating the results and preventing analyses to be carried out. The use of such schemes has allowed results to be obtained and important understandings to be arrived at. However, we note that at the size and time scales of the dynamic deformation of nanowires, there is usually no effective mechanisms for heat to be conducted, convected or radiated out of the system. It is clearly desirable and important to conduct numerical simulations under conditions that do not necessitate artificial schemes for pure numerical reasons. There has been an effort in carrying out simulations at lower strain rates. We describe here some of our recent calculations at strain rates between 10^7 and 10^9 s^{-1}. No temperature controlling algorithms are used, providing a more realistic account of the conditions of the dynamic deformation of nanowires. The focus of the analyses is on the size and rate effects on the constitutive response of Cu nanowires. Parameters varied include loading rate and specimen size.

In the present work, we investigated the size scale and strain rate effects in the tensile deformation of Cu nanowires using MD simulations. The thermal effects and plastic deformation mechanisms are analyzed as the specimen sizes and the applied strain rates are varied. The outline of this paper is as follows. In section II, we introduce some theories and concepts which are used in this paper, i.e. embedded atom method, stress calculation method and the definition of centrosymmetry. In section III, we describe how the simulations are set up. In section IV, the size scale and strain rates effects are discussed in detail from the simulation results. In section V, we quantify the relative errors that may be caused in stress calculation when the kinetic energy term of virial stress is included. Finally, the main results are summarized at the conclusion section VI.

II. ATOMISTIC BACKGROUND

1. Embedded-Atom Method (EAM)

We used the EAM potentials in our MD simulations. EAM is a many-body potential model, first proposed by Daw and Baskes (1984)[11]. Daw et al. (1993) summarized the theory and many applications of EAM[12]. In this method, the energy of the metal is viewed as the energy to embed an atom into the local electron density provided by the remaining atoms of the system. In addition, there is an electrostatic interaction

between atoms. The functional form of the total energy is given by

$$E = \sum_i F_i \left(\sum_{j(\neq i)} \rho_j^a \left(\mathbf{r}_{ij} \right) \right) + \frac{1}{2} \sum_{\substack{i,j \\ (j \neq i)}} \phi_{ij} \left(\mathbf{r}_{ij} \right) \quad (1)$$

where i refers to the atom in question and j refers to a neighboring atom. F is the embedding energy, ρ^a is the spherically averaged atomic density, and ϕ is an electrostatic, two-body interaction. $\mathbf{r}_{ij}$ is distance between atoms i and j.

2. Centrosymmetry

In order to study the plastic deformation in detail, the location and type of defects present must be reliably identified. There are several techniques to separate the defects from the extensive deformation, for example, techniques relying on the electron density, the potential energy, the dislocation density tensor, or the atomic level stress tensor. Kelchner et al. (1998) used a parameter called centrosymmetry to identify defects[13]. This technique is based on the fact that a centrosymmetric material (such as Cu or other FCC metals) will remain centrosymmetric under homogeneous elastic deformation. In centrosymmetric material, each atom has pairs of equal and opposite bonds to its nearest neighbors. As the material is distorted, these bonds will change direction and/or length, but they will remain equal and opposite. When a defect is introduced nearby, this equal and opposite relation no longer holds for all of the nearest neighbor pairs. The centrosymmetry is defined by

$$P = \sum_{i=1,6} \left| \mathbf{R}_i + \mathbf{R}_{i+6} \right|^2 \quad (2)$$

where $\mathbf{R}_i$ and $\mathbf{R}_{i+6}$ are the vectors or bonds corresponding to the six pairs of opposite neighbors in the FCC lattice. Centrosymmetry is zero for homogeneous elastic deformation but nonzero for any plastic deformation of the material. In the above definition, the value of centrosymmetry depends on not only the amount of the plastic deformation but also the lattice constant, which is different from material to material. In this paper, we normalize the centrosymmetry by the lattice constant, i.e.

$$C = \sqrt{P} / a \quad (3)$$

where P is centrosymmetry defined by equation (2), a is the crystal lattice constant. Then the normalized centrosymmetry C only depends on the amount of plastic deformation, while is independent of the type of materials.

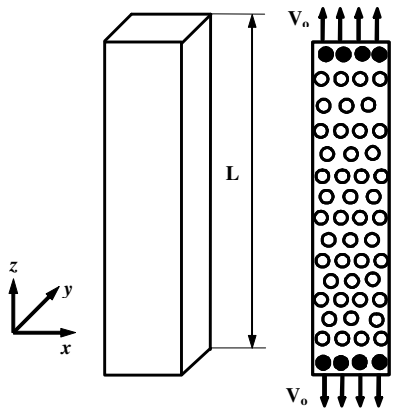

Figure 1: A schematic illustration of the computational model for Cu nanowires. Open circles represent the active atoms and the dark circles represent boundary atoms.

III. COMPUTATIONAL SETUP

We carried out MD simulations of the simple tension of single crystal Cu nanowires, see Fig. 1. The nanowires have free surfaces in the x- and y-directions. The x-, y-, and z-axes are oriented in the [100], [010], and [001] crystalline directions, respectively. The atoms in the specimens are divided into two types. One is the boundary atoms. Constant velocities $\pm V_0$ (equal magnitude and opposite directions) are maintained for these two planes of atoms, effecting loading necessary for the nanowire to deform at a constant nominal strain rate equal to $\dot{\varepsilon} = 2V_0 / L$. The internal atoms simply deform with the boundary atoms. The system is assigned an initial temperature of 300K and is allowed to relax by holding the length of the wire unchanged and by maintaining a constant temperature using the thermostat procedure. The nanowires are not relaxed to a zero stress state and the beginning of deformation is at stress levels of 0.4-1.6 GPa. The calculations continue with a time step of 1 femtosecond until the nanowire fractures. In contrast to some MD simulations reported in the literature where the Nose-Hoover thermostat procedure was used to maintain a constant temperature, no thermal constraints are applied to the specimen during the calculations here; therefore, the temperature rises adiabatically. This more closely simulates the

tensile deformation of a nanowire undergoing high rate deformation.

IV. RESULTS AND DISCUSSION

There are two main aspects we would like to discuss regarding the results, which are the size scale and strain rate effects.

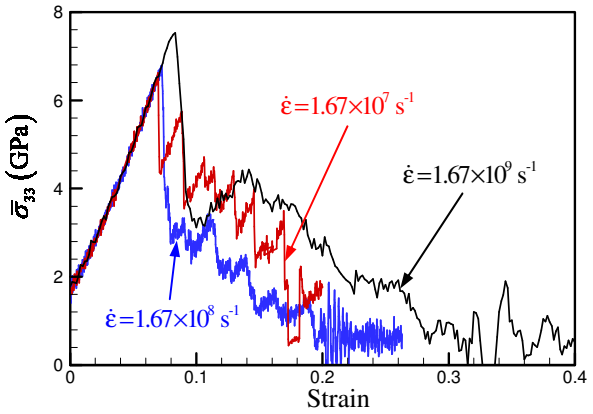

Figure 2: Stress-strain curves of 5×5×60 Cu nanowires at three different strain rates

1. Strain rate effects

Figure 2 shows the stress-strain relations of nanowires at different strain rates, which vary from 1.67×10^7 s^{-1} and 1.67×10^9 s^{-1}.The cross sectional size of the nanowires is 5 lattice constants (1.8×1.8 nm). The stress-strain relations are essentially linear at small strains. The yield stress is the maximum stress in these cases. The curves for different strain rates coincide during the elastic part of the deformation, indicating rate-independence of elastic deformations which is expected. The curves show a rate-independent Young's modulus of 70 GPa for <001> type crystalline directions. The strain at which yielding occurs increases with strain rate. The nanowires yield at greater strains with the increase of strain rates. The yield stress increases from 6.8 GPa to 7.7 GPa as the strain rate increases from 1.67×10^7 s^{-1} and 1.67×10^9 s^{-1}. This influence of rate is due to the dynamic wave effect or phonon drag that impedes the motion of dislocations. Furthermore, this strain rate dependence of ductility is consistent with the experimental results reported by Lu (2001)[5]. Due to the lack of defects and high strain rates, the yield stress for nanowires undergoing dynamic deformation can far exceed that of bulk Cu. The stress-strain curves in Fig. 2 show precipitous drops in stress after yielding. This sharp drop is caused by the initiation of plastic deformation which occurs at different levels of stress for different strain rates. Crystalline slip along {111} planes clearly provides the mechanism for the plastic deformation.

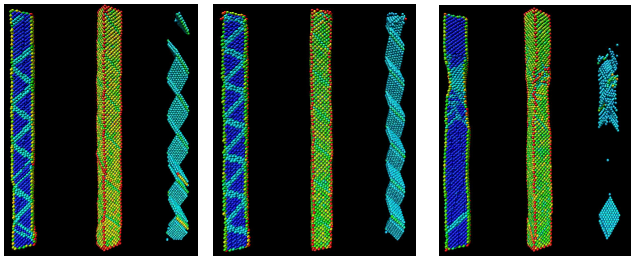

Figure 3: Deformed configurations of Cu nanowires at a strain of 10%; (a) $\dot{\varepsilon}=1.67\times10^7$ s^{-1} ; (b) $\dot{\varepsilon}=1.67\times10^8$ s^{-1} ; and (c) $\dot{\varepsilon}=1.67\times10^9$ s^{-1} . In each picture, the left image shows an internal cross-section, the center images shows a solid view of the wire with all atoms, and the right image shows only atoms involved in defects. Graphics generated using VMD1.7 [14]

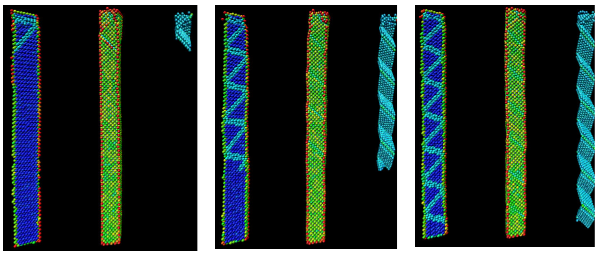

Figure 4: The propagation of slip bands at a strain rate of 1.67×10^8 s^{-1}, (a) $\varepsilon=4.67\%$, (b) $\varepsilon=5.33\%$, and (c) $\varepsilon=6.0\%$. The specimen size is 5×5×60.

Activation of multiple slip planes and cross slip are responsible for the formation of the neck in the specimen (Fig. 3(c)). At the strain rate 1.67×10^8 s^{-1}, regularly distributed, alternating slip bands are clearly observed throughout the specimen (Fig. 3(a,b)). These slip bands are not simultaneously activated. They propagate from one end to the other within a certain period of time (Fig. 4). This novel phenomenon can be explained by the initially uniform but high strain energy state of the nanowire since it is initially pre-strained with fixed ends. At such state, slip planes are likely to be activated by small thermal or mechanical perturbations. The activation of a slip plane at one location can set off a successive, chain-reaction type activation of slip planes down the specimen. This mechanism of plasticity activation is observed for the

strain rates of 1.67×10^{7} s^{-1} and 1.67×10^{8} s^{-1}. The speed at which the active front of the planes propagates along the wire is very high for 1.67×10^{7} s^{-1} and is 355m/s for 1.67×10^{8} s^{-1}. The rapid activation of slip planes across the specimen is responsible for the nearly vertical drop of stress seen following yielding in Fig. 2. The stress-strain curves show oscillatory decreases of stress after the onset of plastic deformation. These oscillations are likely due to successive stages of gradual elastic stretching of temporarily "stationary" lattice structures and rapid plastic slip along the well-defines slip planes. During the elastic stages, straining of the lattice allows strain energy to be accumulated and stored. The stored strain energy allows the activation of slip planes in short, "quick-fire" bursts, leading to relaxation and drop in stress as strain increases. Since specimens deforming at lower strain rates need longer times to "catch up" through further elastic straining, stress decreases are sharper and last longer in time.

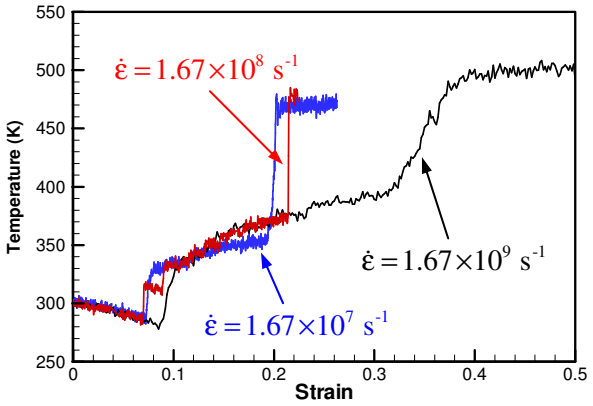

Figure 5: Temperature changes in Cu nanowires of different sizes during the deforming process

The variation of temperature as a function of strain is shown in Fig. 5 for 5×5×60 specimens deformed at different strain rates. The thermal behavior of specimens is similar at the different strain rates. In the elastic deformation stage, temperature decreases slightly as part of the kinetic energy is transformed into potential energy (or strain energy). Subsequently upon yielding, the temperature begins to increase abruptly and continues the upward trend until the nanowires rupture. This temperature increase is primarily due to plastic dissipation but is also due to thermoelastic dissipation at the atomic level. Sharp temperature rises are observed at fracture for $\dot{\varepsilon}=1.67\times10^{7}$ s^{-1} and $\dot{\varepsilon}=1.67\times10^{8}$ s^{-1}, primarily because of the conversion of external work to kinetic energy. The gradual increase of temperature for $\dot{\varepsilon}=1.67\times10^{9}$ s^{-1} at late stages of deformation echoes the more ductile and prolonged deformation at this strain rate.

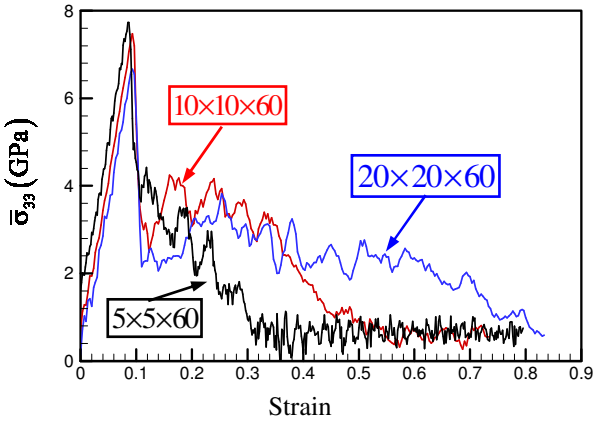

Figure 6: Stress-strain relations for specimens of different sizes, $\dot{\varepsilon}=1.67\times10^{9}$ s^{-1}

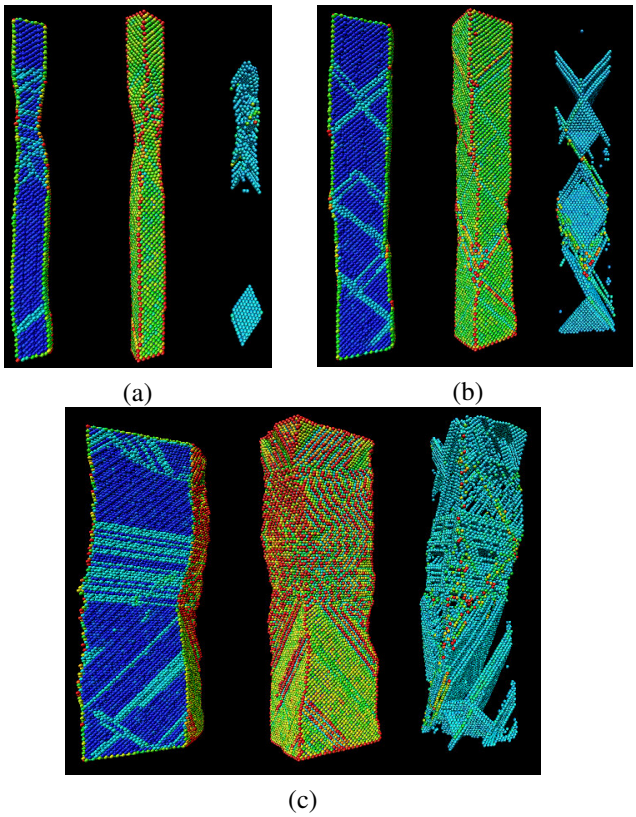

Figure 7: Deformed configurations of Cu nanowires of different sizes ($\dot{\varepsilon}=1.67\times10^{9}s^{-1}$); (a) specimen with a cross-sectional size of 5 lattice spacings $(\varepsilon=9.17\%)$; (b) specimen with a cross-sectional size of 10 lattice spacings, $(\varepsilon=18.3\%)$; and (c) specimen with a cross-sectional size of 20 lattice spacings, $(\varepsilon=23.3\%)$.

2. Size Scale Effects

Figure 6 shows stress-strain curves for specimens of three different sizes at a strain rate of 1.67×10^{9} s^{-1}. The cross-sectional dimensions vary from 5 to 20 lattice constants (or 1.8 to 7.2 nm) and the length is 60 lattice constants (21.7 nm) in all cases. Thinner nanowires support higher stresses and the yield stress decreases with specimen size. However, the Young's modulus remains essentially the same for the different sizes, as the initial, elastic portions of the stress-strain curves are essentially parallel to each other, except for the different amounts of offset at the origin. This offset is due to the uniform pre-stretch applied to the specimens prior to the start of the deformation process. This independence of the Young's modulus on size is different from the findings of Branício who reported that nanowires with larger cross-sections support higher stress levels and have higher values of the Young's modulus[15]. The calculations here also show enhanced ductility at larger sizes. Clearly, this is due to the fact that smaller samples offer fewer opportunities for slip and dislocation motion and larger specimens offer more opportunities for crystalline slip. This effect is clearly seen in Fig. 7. The larger specimen in Fig. 7(c) shows more extensive of slip activation and cross slip.

V. INTERNAL AND EXTERNAL STRESS (TRACTION)

The deformation of nanowires is an intrinsically dynamic process. Proper distinction between internal stress and externally applied stress (traction) must be made. In the current analysis, both the internal stress and externally applied traction are tracked. This allows the fully dynamic nature of the deformation process to be quantified. Historically, one of the most commonly used methods to calculate stress in an MD system is the virial stress. This concept is based on the virial theorem of Clausius[16]. The virial stress includes a kinetic energy part and an interatomic force part[17-19]. Specifically, the average virial stress in the specimen is

$$\bar{\Pi}=\frac{1}{V}\sum_{i}\left(-m_i\dot{\mathbf{u}}_i\otimes\dot{\mathbf{u}}_i+\frac{1}{2}\sum_{j}\mathbf{r}_{ij}\otimes\boldsymbol{f}_{ij}\right) \qquad (4)$$

where, V is the volume of the specimen, m_i is the mass of atom i, $\mathbf{u}_i$ is the displacement of atom i relative to a reference position, $\dot{\mathbf{u}}_i=\mathrm{d}\mathbf{u}_i/\mathrm{d}t$ represents material time derivative of $\mathbf{u}_i$, $\mathbf{r}_{ij}=\mathbf{r}_j-\mathbf{r}_i$, $\mathbf{r}_i$ is the position of i, and $\otimes$ denotes the tensor product of two vectors with $(\mathbf{a}\otimes\mathbf{b})_{\alpha\beta}=a_\alpha b_\beta$ (a_α and b_β are Cartesian components of $\mathbf{a}$ and $\mathbf{b}$ respectively, $\alpha,\beta=1,2,3$). $\boldsymbol{f}_{ij}$ is the interatomic forces applied on atom i by atom j.

Zhou (2002) has shown that the kinetic energy term in the virial stress causes it to violate balance of momentum, if it is interpreted as a form of mechanical stress[20]. The conclusion is that the interatomic force part of the virial stress alone fully constitutes the Cauchy stress. Specifically, for a region with volume Ω around atom i, the average stress is

$$\bar{\boldsymbol{\sigma}}=\frac{1}{2\Omega}\sum_{j(\neq i)}\mathbf{r}_{ij}\otimes\boldsymbol{f}_{ij}\ . \qquad (5)$$

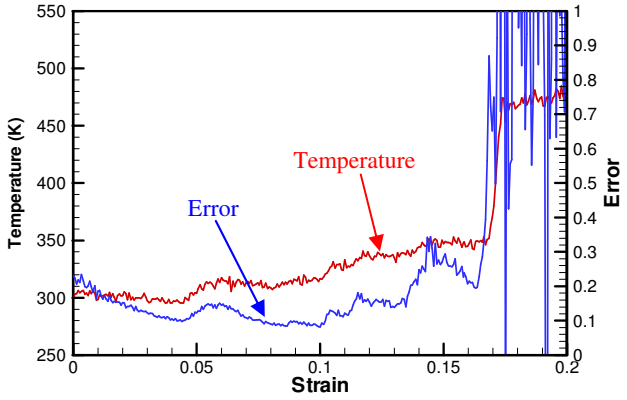

Figure 8: Variation of temperature and the error of stress calculation ($\dot{\varepsilon}=1.67\times10^{8}$ s^{-1})

This new understanding is reflected and used in current analysis. In particular, the analysis focuses on error that may be caused in stress calculation when the kinetic energy term is included. The relative error of stress calculation is defined as the ratio between the kinematic part and interatomic force part in equation (4). More specifically,

$$\text{error}=\frac{\left|\sum_i m_i\left[\left(\dot{\mathbf{u}}_i\right)_3\right]^2\right|}{\left|\bar{\sigma}_{33}\right|} \qquad (6)$$

where $\left(\dot{\mathbf{u}}_i\right)_3$ is the component of $\dot{\mathbf{u}}_i$ in the axial direction of the wire and $\bar{\sigma}_{33}$ is the normal stress component of $\bar{\boldsymbol{\sigma}}$ in the axial direction. It is found that the relative error varies as the deformation progresses (see Fig. 8). At the onset of yielding, the level of error is on the order of 5-10%. However, at large plastic strains,

the error is typically of the order of 20-30% and can exceed 100% toward the late stages of deformation when fracture initiates. Hence, large errors by including the kinetic energy term may prevent one from correctly interpreting the simulation results.

VI. CONCLUSION

Atomistic simulations using embedded atom method were performed for single crystal Cu nanowires. The strain rate and size sale effects were studied. In the elastic deformation stage, the Young's modulus was primarily independent of strain rates and the cross sectional size of specimens. The yield stress (stress at which plastic deformation initiates) decreases with specimen size, while increases with loading rate. On the other hand, ductility increases with specimen size and strain rate. The influences of specimen size are a result of enhanced opportunities for dislocation motion at larger sizes. The influenced of rate are due to the dynamic wave effect or phonon drag that impedes the motion of dislocations.

The analysis also focuses on the variation of deformation mechanisms with specimen size and strain rate. There is a clear transition in deformation mechanism as specimen size is changed. Specifically, when cross-sectional dimensions are on the order of only a few lattice constants, a combination of twinning and slip is observed. At larger cross-sectional sizes (10-20 lattice constants), crystalline slip is primarily responsible for the progression of plastic deformation. Furthermore, a strong strain rate effect is also seen. As strain rate is decreased, a transition of deformation mechanism from combined twining and slip to sequential propagation of slip along well defined and favorably oriented slip planes is observed. Due to the high strain rate, deformation twins are formed during plastic deformation, which serves to reorient the crystal lattice to favor further basal slip. Hence, the combination of twinning and slipping make the specimen more ductile at higher strain rates. The initiation of twins and relaxation of stress make the stress-strain curves display a zigzag of increase and decrease after yielding. At the lower strain rates, a well-structured activation of slip on alternating slip planes is the primary deformation mode.

ACKNOWLEDGEMENTS

This research is supported by NASA Langley Research Center. We would like to thank S. Plimpton for sharing his MD code. We also thank the developer of Visual Molecular Dynamics (VMD) [14]. The snapshots in this paper are created by VMD.

REFERENCES

1. Agräit, N., G. Rubio, and S. Vieira, Physical Review Letters, 1995. **74**(20): p. 3995.
2. Ikeda, H., et al., Physical Review letters, 1999. **82**(14): p. 2900.
3. Rubio-Bollinger, G., et al., Physical Review Letters, 2001. **87**(2): p. 026101.
4. Mehrez, H. and S. Ciraci, Physical review B, 1997. **56**(19): p. 12632.
5. Lu, L., S.X. Li, and K. Lu, Scripta Materialia, 2001. **45**: p. 1163.
6. Ikeda, H., et al., Physical Review Letters, 1999. **82**(14): p. 2900.
7. Branicio, P.S. and J.-P. Rino, Physical Review B (Condensed Matter), 2000. **62**(24): p. 16950.
8. Horstemeyer, M.F. and M.I. Baskes, Transactions of the ASME. Journal of Engineering Materials and Technology, 1999. **121**(2): p. 114.
9. Nose, S., Mol. Phy., 1984. **52**(2): p. 255.
10. Hoover, W.G., Physical Review A, 1985. **31**(3).
11. Daw, M.S. and M.I. Baskes, Physical Review B (Condensed Matter), 1984. **29**(12): p. 6443.
12. Daw, M.S., S.M. Foiles, and M.I. Baskes, Material Science Reports, 1993. **9**(7-8): p. 251.
13. Kelchner, C.L., S.J. Plimpton, and J.C. Hamilton, Physical Review B (Condensed Matter), 1998. **58**(17): p. 11085.
14. Humphrey, W., A. Dalke, and K. Schulten, J. Molec. Graphics, 1996. **14**: p. 33.
15. Branício, P.S. and J.P. Rino, Physical Review B : Condensed Matter, 2000. **62**(24): p. 16950.
16. Clausius, R., Phil. Mag., 1870. **40**: p. 122.
17. Tsai, D.H., J. Chem. Phys., 1979. **70**: p. 1375.
18. Rowlinson, J.S. and B. Widom. 1982, Oxford: Clarendon Press. 85.
19. Swenson, R.J., Am. J. Phys., 1983. **51**: p. 940.
20. Zhou, M., Submitted to Physical Review B, 2002.